Journal of Thermal Analysis and Calorimetry (2023) 148:12987–13001
https://doi.org/10.1007/s10973-023-12421-9

# Mixing phase behavior of trilaurin and monounsaturated triacylglycerols based on palmitic and oleic fatty acids

**Jorge Macridachis[1] · Laura Bayés-García[1] · Teresa Calvet[1]**

Received: 14 December 2022 / Accepted: 20 July 2023 / Published online: 7 August 2023


## Abstract

Differential scanning calorimetry and X-ray diffraction were used to examine the mixing phase behavior of LLL (trilaurin or 1,2,3-trilauroyl-glycerol) and POP (1,3-dipalmitoyl-2-oleoyl-glycerol), PPO (1,2-dipalmitoyl-3-oleoyl-rac-glycerol), or the 50POP/50PPO blend able to form a molecular compound. This research aims to provide an insight into the molecular interactions ruling the physical behavior of fat blends of lauric (i.e., coconut oil) and non-lauric lipids (cocoa butter, palm oil, etc.). The results showed eutectic behavior and no mutual solubility of triacylglycerols in stable LLL/POP and LLL/PPO mixtures. Applying high-rate cooling treatments had a positive effect on miscibility, but the high incompatibility of the components due to differences in length and degree of unsaturation of fatty acids was still evident in metastable polymorphs. In ternary LLL/(50POP/50PPO) mixtures, on the other hand, molecular compound β-2L crystals formed by POP and PPO showed to favor the solubility of LLL as compared to the binary systems. Accordingly, promoting the presence of triacylglycerols forming molecular compound in specific fat blends may help reducing eutectic or incompatible interactions among triacylglycerol molecules in the solid state. These lead to phase separation and are a major cause of the restricted applicability of lauric oils in the confectionery and chocolate industries.

**Keywords** Thermal analysis · Polymorphism · Crystallization · Triacylglycerol · Mixing behavior

## Introduction

The crystalline properties and solid-phase behavior of triacylglycerols (TAGs) contained in natural fats and oils determine the melting point, texture, and shelf-life of diverse pharmaceutical, cosmetic, and food products. According to the lateral packing of TAGs during crystallization, α, β′, and β polymorphs may be formed, which correspond to the hexagonal (H), orthorhombic perpendicular ($O_{\perp}$), and triclinic parallel ($T_{//}$) subcells, respectively [1]. In turn, the longitudinal packing of TAGs defines the chain-length structure (CLS), which is typically double (2L) or triple (3L). In this connection, β′ crystals are preferred in spreadable foods like margarine, whereas β-3L crystals confer its unique melting behavior and texture to chocolate. Three mixing states can occur in TAG blends, namely complete solid solution (ss), phase separation or eutectic interaction, and molecular compound (MC) formation [2]. As an example, the eutectic interaction in PPP/POP (with P and O being palmitic and oleic acids, respectively), PPP/PPO, and PPP/POO mixtures [3–5] or the molecular compound formed by POP and PPO at a 1:1 ratio [6] rule the crystallization and melting behavior of palm oil and, therefore, play a key role in the industrial fractionation of this oil and the formulation of novel palm-based products.

Lauric oils represent a group of edible lipids mainly constituted by trisaturated TAGs rich in lauric (L), myristic (M), and capric acids (C). Thus, LLL, CLL, LLM, or CCL account for ~ 90% and ~ 60% of the total mass of coconut and palm kernel oils, respectively [1, 7]. These oils are fractionated, hydrogenated, interesterified, and/or blended to produce margarine, spreads, and pastry [8]. In confectionery, compound coatings formulated with lauric-based cocoa butter substitutes (CBS) are used to enrobe snacks, biscuits, or bakery products when chocolate is not suitable in terms of economic feasibility, processing conditions, or functionality of the manufactured foods [9]. In this sense, lauric-CBS provide good oxidative stability,

✉ Jorge Macridachis
jmacridachis@ub.edu

[1] Departament de Mineralogia, Petrologia i Geologia Aplicada, Facultat de Ciències de la Terra, Universitat de Barcelona, Martí i Franquès s/n, 08028 Barcelona, Spain

quick solidification, excellent gloss, and a steep melting profile [10, 11].

Due to differences in molecular size and degree of unsaturation of the TAG components, mixtures of lauric and non-lauric lipids tend to show eutectic mixing behavior. This is the case of blends of palm kernel oil and its hard fraction with palm oil or palm stearin [12, 13], or blends of coconut oil and palm stearin [14]. Eutectic formation results in a depression in melting point and a lower hardness, which may be advantageous to provide melt-away properties to candy centers or fat fillings [15], or a quicker melting to table margarine [16]. However, the functionality of end products may be in some cases compromised, with chocolate being the most industrially relevant example. Cocoa butter (CB), rich in POP, POS, and SOS (with S being stearic acid) and lauric-CBS are immiscible at almost all ratios in β-3L and β′-2L forms, respectively [17]. This limits the incorporation of CB into CBS to a maximum of 5%, which results in poor chocolate-like properties [18], for example, in terms of flavor.

Despite the relevance of the mixing interactions between lauric and non-lauric lipids in the functionality of foodstuffs, studies on model TAG mixtures addressed to unveil the polymorphism and miscibility properties of blends with such configuration are scarce in the literature [19]. Yoshikawa et al. investigated LLL/SOS mixtures to provide a molecular insight into the incompatible properties of lauric-CBS and CB under metastable conditions and in most stable polymorphs [20]. The same authors found that the molecular compound of SOS and OSO promoted the direct crystallization of β-2L (LLL) in LLL/SOS/OSO mixtures [21]. Molecular compounds may help, therefore, avoid the characteristic loss of gloss and whitish streaks of fat bloom in compound coatings based on lauric-CBS, which is in part due to β′ to β transitions of TAGs containing lauric acid during storage.

Improving our knowledge about the mixing interactions of LLL and TAGs differing in fatty acid constituents, degree of unsaturation, or polymorphism through the construction of phase diagrams helps to understand complex fat blends including lauric oils and design lipid structuring strategies that improve the functionality of related food products or industrial processes. This study reports on the polymorphic and mixing behavior of mixtures including LLL and the monounsaturated POP and PPO, which are found in edible lipids like CB, lard, or palm and olive oils [22–24]. The phase diagrams of LLL/POP, LLL/PPO, and LLL/POP/PPO (with POP/PPO at an equimolecular ratio to promote molecular compound formation) mixtures after long-time stabilization were determined. In addition, their polymorphic crystallization, transformation, and phase behavior were also investigated during the application of dynamic thermal treatments.

## Experimental

1,2,3-trilauroyl-glycerol or trilaurin (LLL), 1,3-dipalmitoyl-2-oleoyl-glycerol (POP), and 1,2-dipalmitoyl-3-oleoyl-rac-glycerol (PPO) of purity ≥ 99% were provided by Larodan AB (Solna, Sweeden) and used without further treatments.

To prepare the binary mixtures LLL/POP and LLL/PPO, the components were blended in the molten state at 5–10% molar mass intervals and homogenized for several minutes using a vortex mixer. The samples were sealed in amber glass vials with a nitrogen atmosphere and kept at − 20 °C until use. In LLL/POP/PPO mixtures, a constant 1:1 ratio of POP and PPO was maintained at all compositions to promote molecular compound formation. Thus, a stock 50POP/50PPO mixture was prepared in the first place by blending the molten components and stirring. The same was then combined with LLL following the same procedure as in binary mixtures.

Thermal analyses were performed by differential scanning calorimetry (DSC) with a PerkinElmer DSC8000 calorimeter working under a nitrogen flow of 20 $cm^3$ $min^{-1}$ at atmospheric pressure. The equipment was calibrated by means of the melting temperature ($T_m$, °C) and enthalpy ($\Delta H$, J $g^{-1}$) of indium and *n*-decane standards heated at 2 °C $min^{-1}$. Samples (4–4.4 mg) were placed into 50 µL aluminum pans and hermetically sealed. An empty pan served as a reference. Pyris software was used to process DSC curves and obtain the peak top temperatures ($T_{top}$) and $\Delta H$ of the thermal events observed. A correction described elsewhere [25] was applied to estimate $T_{top}$ of the events detected during thermal treatments at rates different from 2 °C $min^{-1}$ (calibration rate). The samples were analyzed in triplicate and the standard error of temperature and energy values was calculated by the Student's method approximation to attain a 95% confidence interval.

To construct the stable phase diagrams of the mixtures, samples contained in sealed aluminum pans and Lindeman glass capillaries were first subjected to a thermal incubation process consisting of 5 days at 37 °C, after which the temperature was lowered to 27 °C. After 9 months, in the case of LLL/POP and LLL/PPO mixtures, and 6 to 12 months, in the case of LLL/(50POP/50PPO) mixtures, the melting behavior of the samples was evaluated by DSC during a heating treatment from 10 °C until complete melting at 2 °C $min^{-1}$.

To study the polymorphic and mixing behavior of the mixtures under metastable conditions, the thermal protocol applied in DSC experiments consisted of fast cooling from the melt to − 30 °C at 25 °C $min^{-1}$, holding for 1 min at this temperature, and reheating at 5 °C $min^{-1}$.

To achieve the polymorphic identification, the same thermal treatments used during DSC studies were applied in X-ray diffraction (XRD) experiments.

The XRD study of mixtures subjected to thermodynamic stabilization was carried out with a PANalytical X'Pert Pro MPD powder diffractometer with the Debye–Scherrer Geometry and equipped with a hybrid monochromator and a PIXcel detector. The control of temperature during the heating treatment was possible through an Oxford Cryostream Plus 220 V. During the experiments, the 1 mm diameter Lindemann glass capillary containing the sample was rotated around its axis to prevent interference in the results derived from a preferential crystalline orientation. XRD patterns were acquired in the 2θ range from 1° to 28°. A step size of 0.013° and a measuring time of 150 s was applied to all the samples. Data analysis was possible through X'Pert Highscore V2.2e software.

Mixtures subjected to dynamic thermal treatments were investigated by synchrotron X-ray diffraction (SR-XRD) at beamline BL11-NCD-SWEET of the ALBA Synchrotron facility (Cerdanyola del Vallès, Barcelona, Spain) at 12.4 keV. The small- (SAXD) and wide-angle X-ray diffraction (WAXD) data were recorded by a Pilatus 1 M detector (pixel size of 172 µm X 172 µm) and a LX255-HS Rayonix detector (pixel size of 88 mm X 88 µm), respectively.

**Table 1** Diffraction data of LLL, PPO, POP, and $MC_{POP/PPO}$ polymorphs [6, 26–29]

| | CLS | LS/nm | SS/nm |
|---|---|---|---|
| *LLL*[26] | | | |
| α | 2L | 3.5 | 0.42 |
| β′ | 2L | 3.2 | 0.42, 0.38 |
| β | 2L | 3.1 | 0.46, 0.39, 0.38 |
| *PPO*[27,28] | | | |
| Sub- α | 2L | 4.1 | 0.41, 0.37 |
| $\alpha_2$ | 2L | 4.98 → 3.9 | 0.41 |
| $\alpha_1$ | 3L | 7.8 | 0.41 |
| $\beta'_2$ | 2L | 4.2 | 0.41, 0.38 |
| $\beta'_1$ | 3L | 6.7 | 0.41, 0.38 |
| *POP*[29] | | | |
| α | 2L | 4.7 | 0.42 |
| γ | 3L | 6.5 | 0.47, 0.45, 0.39, 0.36 |
| δ | 3L | 6.3 | 0.43, 0.41, 0.38 |
| $\beta'_2$ | 2L | 4.2 | 0.44, 0.42, 0.40 |
| $\beta'_1$ | 2L | 4.2 | 0.43, 0.41, 0.40 |
| $\beta_2$ | 3L | 6.1 | 0.46, 0.41, 0.39, 0.38, 0.37 |
| $\beta_1$ | 3L | 6.1 | 0.46, 0.41, 0.39, 0.37, 0.36 |
| $MC_{POP/PPO}$[6] | | | |
| α | 2L | 4.6 | 0.43, 0.42 |
| B′ | 2L | 4.2 | 0.43, 0.39 |
| β | 2L | 4.1 | 0.46, 0.40, 0.38 |

*LS* long spacing; *SS* short spacing

The *q*-axis of SR-SAXD patterns was calibrated with silver behenate and that of SR-WAXD patterns was calibrated with $Cr_2O_3$. During the SR-XRD study, a linkam stage was used to control the temperature of the sample (2 mm thick) contained in an aluminum cell sealed with kaptom film windows. SR-SAXD and SR-WAXD patterns were taken simultaneously at 12 s intervals during cooling and heating treatments. Data analysis was performed through Igor Pro V6.3.7.2 software.

## Results

### Binary mixtures LLL/POP

#### Mixtures subjected to thermodynamic stabilization

Diffraction data used for the polymorphic identification in this study are depicted in Table 1 [6, 26–29]. Figure 1a shows the XRD patterns of LLL/POP mixtures taken at 10 °C after 9 months of thermal incubation. The phase diagram constructed from the DSC data ($T_{top}$ of melting) of mixtures heated from 10 °C to complete melting at 2 °C $min^{-1}$ is shown in Fig. 1b (see detailed DSC data in Fig. S1 of Supplementary Information).

XRD patterns confirmed stable β-2L (LLL) (SAXD peak at 3.1 nm and WAXD peaks at 0.46, 0.38, and 0.37 nm) and $\beta_1$-3L (POP) (002 reflection at 3.0 nm in SAXD patterns and WAXD reflections at 0.46, 0.40, 0.38, 0.37, and 0.36 nm) forms in all samples. Their concurrent presence at all compositions indicated a solubility of each TAG in the solid phase of the other < 5%. As shown by the diagram, in mixtures with LLL content from 95 to 35%, $\beta_1$-3L (POP) melted first at ~ 37 °C and then β-2L (LLL) followed (~ 46 °C to ~ 40 °C). In mixtures with LLL content ≤ 30%, β-2L (LLL) and β-3L (POP) melting peaks were not distinguished by DSC and, thus, no accurate eutectic point was identified. However, the trend shown by the liquidus curve in the diagram pointed to a composition with ≤ 20% LLL content. The XRD data taken when heating the 10LLL/90POP mixture (data not shown) confirmed the earlier vanishing of β-2L (LLL). This suggested a eutectic composition with 20–10% LLL content.

#### Mixtures subjected to dynamic thermal treatments of cooling and reheating

Figure 2 shows the map of crystalline phases identified in LLL/POP mixtures by DSC and SR-XRD when cooled from the melt to − 30 °C at 25 °C $min^{-1}$ and reheated at 5 °C $min^{-1}$. At the end of cooling, solid solutions (ss) (denoted with capital letters) and crystalline phases linked to the major TAG present (lower case letters) occurred at

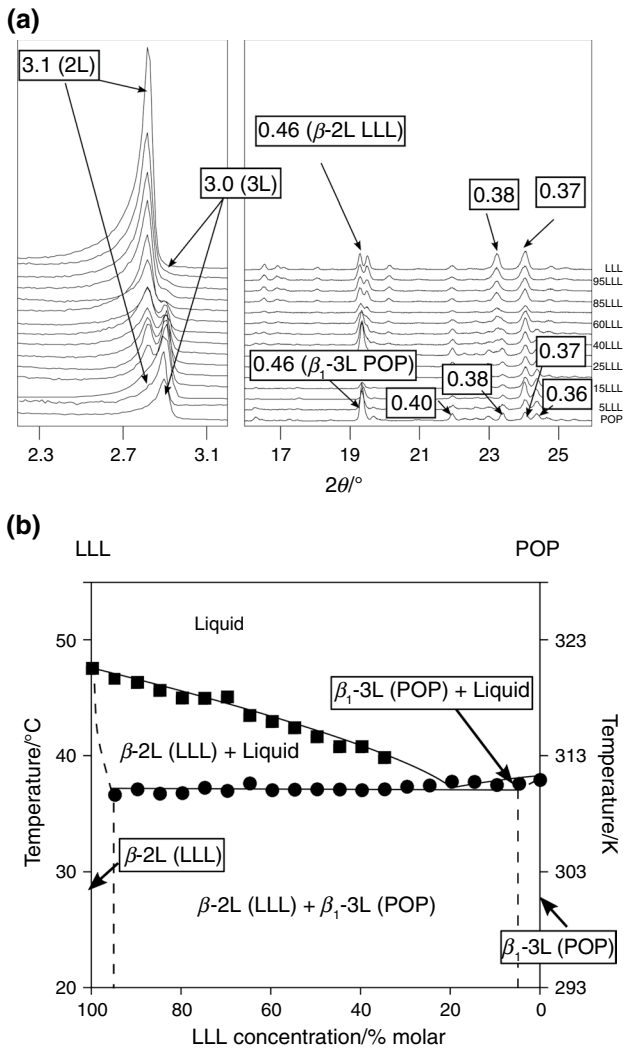


**Fig. 1** LLL/POP mixtures stabilized at 37 °C for 5 days and at 27 °C for 9 months. **a** XRD patterns obtained at 10 °C. *d*-spacing values are given in nm. **b** Phase diagram obtained when heating the mixtures at 2 °C min.$^{-1}$

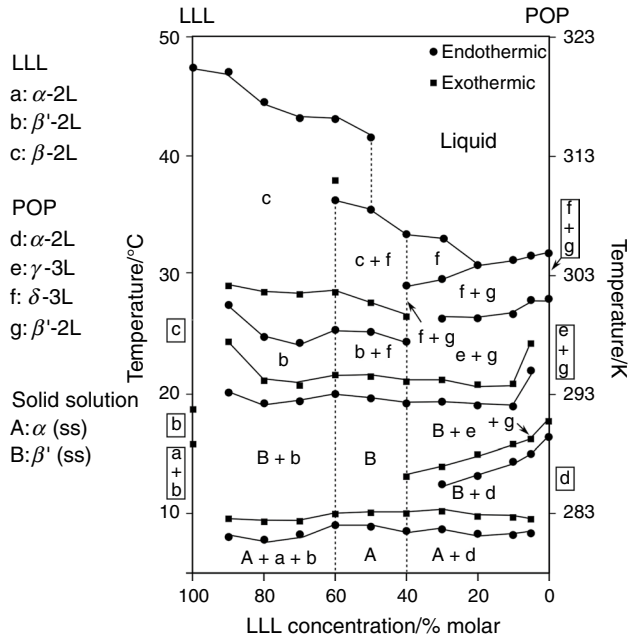


**Fig. 2** Phase behavior observed for LLL/POP mixtures heated at 5 °C min$^{-1}$ after cooling at 25 °C min$^{-1}$. Delimited areas correspond to polymorphic domains between transitions experimentally determined

almost all compositions. The identification of solid solutions was possible due to the occurrence of SAXD peaks with spacing values different from those reported in the literature for LLL or POP polymorphs. As depicted in the figure, the varying polymorphic crystallization behavior of the mixtures as a function of the LLL/POP ratio when cooling, governed the distinct transformation behavior displayed when reheating.

Figure 3a shows the DSC and SR-XRD data obtained for the 90LLL/10POP mixture. The DSC peak detected at ~4 °C on cooling involved the crystallization of β′-2L (LLL) (SAXD peak at 3.3 nm, and WAXD peaks at 0.44 and 0.39 nm spotted at ~ − 1 °C), α-2L (LLL) (3.6 and 0.41 nm), and one α (ss) (4.1 and 0.41 nm) with a long spacing value not ascribed to LLL or POP forms. The formation of α (ss) grew toward the equimolecular mixture until being the only form detected (see SR-XRD data of the 60LLL/40POP mixture in Fig. 3b). However, in POP-rich mixtures, α-2L (POP) (SAXD peak at 4.6 nm and WAXD peak at 0.41 nm detected at ~ − 6 °C in SR-XRD data of the 20LLL/80POP mixture in Fig. 3c) crystallized before α (ss). The high amount of α-2L (POP) formed near the pure POP sample impeded the detection of other forms present in the mixtures just by SR-XRD (see data of the 5LLL/95POP mixture in Fig. 3d).

When reheating LLL-rich mixtures, which showed α (ss), α-2L (LLL), and β′-2L (LLL) crystals on cooling, α (ss) and α-2L (LLL) melted first, after which β′ (ss) crystallized. This led to endothermic and exothermic DSC peaks at ~8 and ~9 °C, respectively, in the 90LLL/10POP mixture (Fig. 3a). Alongside, reflections at 4.1 and 3.6 nm faded, and that at 3.3 nm grew in related SAXD patterns at ~9 °C. Moreover, β′ (ss) reflections at 0.44, 0.42, and 0.39 nm arose in WAXD patterns. On further heating, the one at 3.3 nm shifted to 3.2 nm and WAXD patterns at 22 °C showed changes in the β′ subcell: a peak grew at 0.40 nm and that at 0.39 nm strengthened and moved to 0.38 nm. This was due to the melting of β′ (ss) and the next occurrence of β′-2L (LLL), which led to DSC peaks at ~20 °C and ~24 °C. Later on, this form melted and β-2L (LLL) crystallized (SAXD peak at 3.1 nm and WAXD peaks at 0.46, 0.39, and 0.37 nm).

The single α (ss) obtained in mixtures near the equimolecular composition during cooling, when reheating it transited via melt-mediation to β′ (ss). In the 60LLL/40POP

mixture (see Fig. 3b), β′ (ss) melted at ~ 20 °C and β′-2L (LLL) and δ-3L (POP) (002 reflection in SAXD patterns at 3.3 nm and WAXD peaks at 0.43, 0.40, and 0.37 nm) crystallized. β′-2L (LLL) reflections vanished a few degrees above, in line with the DSC melting peak spotted at ~ 25 °C. The next formation of β-2L (LLL) was slowed down by the presence of POP, and related SR-XRD peaks were only seen once δ-3L (POP) vanished (DSC melting peak at ~ 36 °C).

POP-rich blends showed consecutive α (ss) → β′ (ss) and α-2L (POP) → γ-3L (POP) transitions when reheating. In the 20LLL/80POP mixture (see Fig. 3c), the last one led to endothermic and exothermic events at ~ 13 and ~ 15 °C in the DSC curve. γ form was identified in SR-XRD patterns through WAXD peaks at 0.47, 0.45, and 0.39 nm and SAXD peak at 3.5 nm (002 reflection). β′ (ss) melted next and a new form with a reflection at 4.2 nm occurred (DSC peaks at ~ 19 and ~ 21 °C). The same was attributed to β′-2L (POP) through WAXD peaks grown at 0.44, 0.42, and 0.39 nm at a close temperature but it was unclear whether this form corresponded to $\beta'_2$ or $\beta'_1$ of POP. Thus, as illustrated in Fig. 2, the formation of β′-2L (POP) from β′ (ss) was favored over β′-2L (LLL) in POP-rich blends and the opposite occurred in LLL-rich ones. Once β′-2L (POP) crystallized, the DSC curves of the POP-rich mixtures showed the γ-3L → melt → δ-3L transformation of POP at ~ 26 °C and the next melting of β′-2L (POP) and δ-3L (POP) at ~ 31 °C. The detection of DSC events involving POP and solid solutions even in the 5LLL/95POP mixture (see Fig. 3d), evidenced the great tendency to eutectic interaction of metastable LLL and POP.

## Binary mixtures LLL/PPO

### Mixtures subjected to thermodynamic stabilization

XRD data obtained at 10 °C for LLL/PPO mixtures (Fig. 4a) showed stable β-2L (LLL) and $\beta'_1$-3L (PPO) forms at all compositions. In addition, the melting behavior monitored when heating the samples at 2 °C $min^{-1}$, which is depicted in the diagram of Fig. 4b (see detailed data in Fig. S2) confirmed similar eutectic behavior to that of LLL/POP mixtures. LLL-rich mixtures showed the successive melting of $\beta'_1$-3L (PPO) and β-2L (LLL), and a solubility of PPO in LLL < 5%. The decreasing melting temperature of β-2L (LLL) toward the pure PPO sample caused the overlapping of the two DSC melting peaks in mixtures with LLL content < 25%. Therefore, no eutectic point was exactly determined by DSC. The XRD patterns taken when heating the 10LLL/90PPO mixture showed the only presence of $\beta'_1$-3L (PPO) before the vanishing of all reflections (data not shown), which suggested a eutectic composition with 20–10% LLL content. As in LLL/POP mixtures, LLL did not dissolve in the mixed-acid TAG at the lowest concentration tested.

### Mixtures subjected to dynamic thermal treatments of cooling and reheating

Figure 5 depicts the map of crystalline phases determined for LLL/PPO mixtures during the heating process at 5 °C $min^{-1}$ succeeding the fast-cooling treatment at 25 °C $min^{-1}$. No complete miscibility was observed at any composition, and solid solutions together with phases very rich in either LLL or PPO determined the polymorphic behavior when cooling and reheating.

The crystallization of β′-2L (LLL), α-2L (LLL), and α (ss) in LLL-rich mixtures when cooling led to single broad peaks in the DSC curves. In the 90LLL/10PPO mixture (see experimental data in Fig. 6a), typical α and β′ WAXD reflections occurring at ~ − 1 °C were together with two strong SAXD reflections at 3.5 and 3.3 nm linked to α-2L (LLL) and β′-2L (LLL), respectively. The small signal detected at around 3.8 nm and not associated with the pure TAGs was probably due to α (ss). Reducing the LLL content hindered the inclusion of PPO in α (ss). Thus, as shown for the 60LLL/40PPO mixture in Fig. 6b, no LLL forms but $\alpha_2$-2L (PPO) crystallized before α (ss). This led to a reflection at 4.9 nm in SAXD patterns at ~ − 1 °C, which shifted to 4.2 nm on further cooling. When reaching -21 °C, the new WAXD peak at 0.37 nm indicated a α → sub-α transition. Given its absence in mixtures with higher LLL content, this event probably only involved $\alpha_2$-2L (PPO).

The crystallization of $\alpha_2$-2L (PPO) and α (ss) in PPO-rich mixtures, with the amount of $\alpha_2$-2L (PPO) increasing toward the pure PPO sample, led to discernible exothermic peaks in the DSC curves (see data of mixtures with 40% and 5% LLL content in Fig. 6c and d, respectively). In the corresponding SR-XRD patterns, one may notice a visibly wider SAXD peak of α (ss) at 3.9 nm. Probably, $\alpha_1$-3L (PPO), with a characteristic 002 reflection at 3.9 nm, also crystallized.

During the heating treatment of mixtures very rich in LLL (see experimental data of the 90LLL/10PPO mixture in Fig. 6a), α (ss) and α-2L (LLL) melted at ~ 9 °C, after which β′ (ss) crystallized. In the next exothermic event at ~ 20 °C, β′ (ss) and β-2L (LLL) vanished, and β-2L (LLL) occurred before the final melting. As to mixtures with 60–20% LLL content, which showed sub-α (PPO) and α (ss) at the end of cooling, they behaved similarly when reheating. According to SR-XRD data at ~ 0 °C (see Fig. 6b and c), sub-α (PPO) transited to $\alpha_1$-3L (PPO) in the first place. Thus, the sub-α peak at 0.37 nm vanished from WAXD patterns, and the SAXD peak at 3.9 nm grew from that at 4.2 nm. This transition was not detected by DSC but endothermic and exothermic peaks corresponding to the next α (ss) → melt → β′ (ss) transformation occurred at ~ 9 °C. The

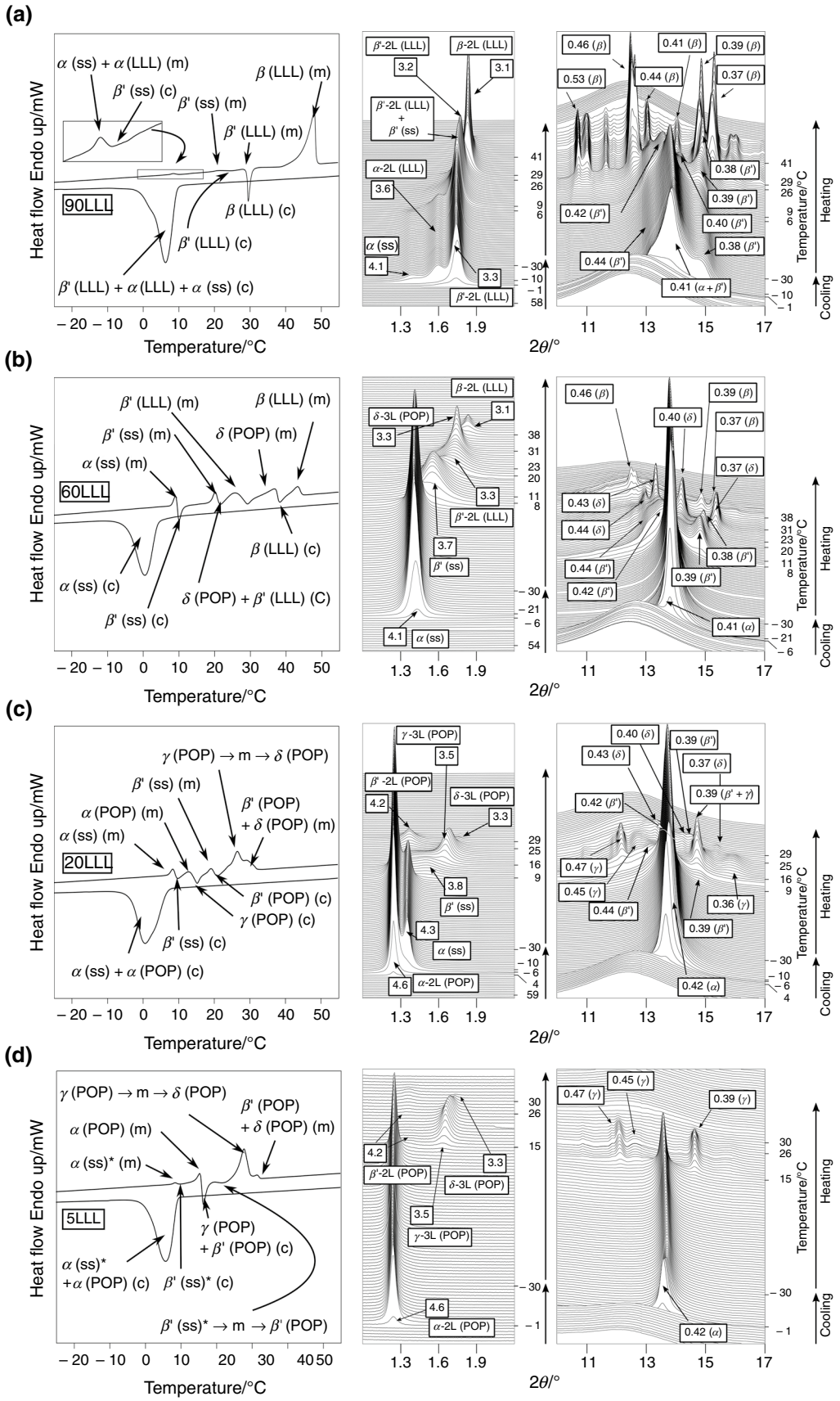
(a)
α (ss) + α (LLL) (m)
β' (ss) (c)
β' (ss) (m)
β (LLL) (m)
β' (LLL) (m)
90LLL
β (LLL) (c)
β' (LLL) (c)
β' (LLL) + α (LLL) + α (ss) (c)
Heat flow Endo up/mW
Temperature/°C
β'-2L (LLL)
β-2L (LLL)
3.2
3.1
β'-2L (LLL) + β' (ss)
α-2L (LLL)
3.6
α (ss)
4.1
3.3
β'-2L (LLL)
0.46 (β)
0.41 (β)
0.39 (β)
0.53 (β)
0.44 (β)
0.37 (β)
0.38 (β')
0.39 (β')
0.42 (β')
0.40 (β')
0.44 (β')
0.38 (β')
0.41 (α + β')
Temperature/°C
Heating
Cooling
2θ/°
(b)
β' (LLL) (m)
β (LLL) (m)
β' (ss) (m)
δ (POP) (m)
α (ss) (m)
60LLL
β (LLL) (c)
α (ss) (c)
δ (POP) + β' (LLL) (C)
β' (ss) (c)
β-2L (LLL)
δ-3L (POP)
3.1
3.3
3.3
β'-2L (LLL)
3.7
β' (ss)
4.1
α (ss)
0.46 (β)
0.40 (δ)
0.39 (β)
0.37 (β)
0.37 (δ)
0.43 (δ)
0.44 (δ)
0.38 (β')
0.44 (β')
0.39 (β')
0.42 (β')
0.41 (α)
(c)
γ (POP) → m → δ (POP)
β' (ss) (m)
α (POP) (m)
β' (POP) + δ (POP) (m)
α (ss) (m)
20LLL
β' (POP) (c)
γ (POP) (c)
β' (ss) (c)
α (ss) + α (POP) (c)
γ-3L (POP)
3.5
β' -2L (POP)
δ-3L (POP)
4.2
3.3
3.8
β' (ss)
4.3
α (ss)
4.6
α-2L (POP)
0.40 (δ)
0.39 (β')
0.43 (δ)
0.37 (δ)
0.39 (β' + γ)
0.42 (β')
0.47 (γ)
0.45 (γ)
0.44 (β')
0.36 (γ)
0.39 (β')
0.42 (α)
(d)
γ (POP) → m → δ (POP)
β' (POP) + δ (POP) (m)
α (POP) (m)
α (ss)* (m)
5LLL
γ (POP) + β' (POP) (c)
α (ss)* + α (POP) (c)
β' (ss)* (c)
β' (ss)* → m → β' (POP)
4.2
3.3
β'-2L (POP)
δ-3L (POP)
3.5
γ-3L (POP)
4.6
α-2L (POP)
0.47 (γ)
0.45 (γ)
0.39 (γ)
0.42 (α)

◂**Fig. 3** LLL/POP mixtures. DSC (left) and SR-XRD data (right) of **a** 90LLL/10POP, **b** 60LLL/40POP, **c** 20LLL/80POP, and **d** 5LLL/95POP mixtures heated at 5 °C $min^{-1}$ after cooling at 25 °C $min^{-1}$. (c): crystallization; (m): melting. *Not detected by SR-XRD. *d*-spacing values are given in nm

close long spacing value of β′ (ss) and the preceding α (ss) (3.8–3.9 nm) hindered its distinction from $\alpha_1$-3L (PPO) in SAXD patterns. On further heating, $\alpha_1$-3L (PPO) transited to $\beta'_2$-2L (PPO). DSC endothermic and exothermic events in the 40LLL/60PPO mixture between 16 and 19 °C (Fig. 6c) showed the melt-mediated nature of this transition. At this point, only β′ was detected in WAXD patterns, and a SAXD peak at 4.1 nm raised from that at 3.9 nm. Thus, β′ (ss) and $\beta'_2$-2L (PPO) were present until β′ (ss) melted and β-2L (LLL) occurred. Then, $\beta'_2$-2L (PPO) and β-2L (LLL) melted sequentially.

Sub-α (PPO) → α (PPO) and $\alpha_2$-2L (PPO) → $\alpha_1$-3L (PPO) transitions were first identified in mixtures near the pure PPO sample. In the 5LLL/95PPO blend (see experimental data in Fig. 6d), the second one led to an endothermic peak in the DSC curve at ~13 °C. Then, $\alpha_1$-3L (PPO) melted at ~19 °C, and $\beta'_2$-2L (PPO) and $\beta'_1$-3L (PPO) crystallized. SAXD peaks at 4.2 and 3.4 nm (002 reflection) and typical β′ WAXD reflections were detected at around this temperature. The melting of α (ss) was not detected by DSC but that of β′ (ss) was still visible at ~22 °C (denoted by a white arrow). The next endothermic events were due to the $\beta'_2$-2L (PPO) → $\beta'_1$-3L (PPO) transition (strengthening of the SAXD peak at 3.4 nm at the expense of that at 4.2 nm) and $\beta'_1$-3L melting. The final melting stage determined by $\beta'_1$-3L (PPO) and β-2L (LLL) in mixtures with LLL content < 20% and ≥ 20%, respectively, led to a eutectic minimum (see Fig. 5) in line with the eutectic composition at 20–10% LLL content shown by stable LLL/PPO mixtures.

## Ternary mixtures LLL/(50POP/50PPO)

### Mixtures subjected to thermodynamic stabilization

Diffraction data acquired at 10 °C after 12 months of thermal incubation is shown in Fig. 7a. The phase diagram constructed from the DSC curves of samples heated at 2 °C $min^{-1}$ is depicted in Fig. 7b (see additional DSC data in Fig. S3).

All POP and PPO formed molecular compound in the 50POP/50PPO mixture (SAXD peak at 4.2 nm and WAXD

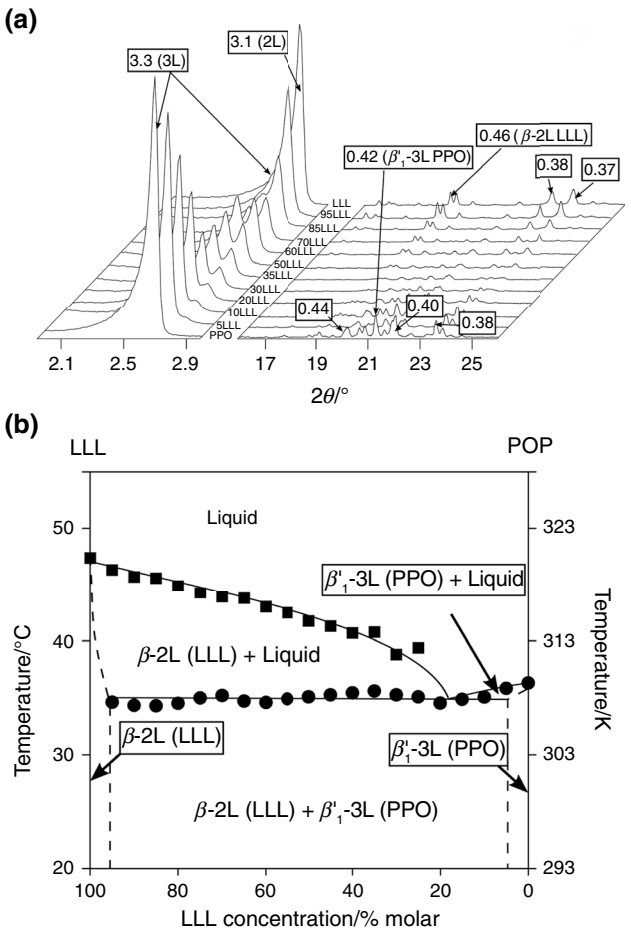


**Fig. 4** LLL/PPO mixtures stabilized at 37 °C for 5 days and at 27 °C for 9 months. **a** XRD patterns obtained at 10 °C. *d*-spacing values are given in nm. **b** Phase diagram obtained when heating the mixtures at 2 °C $min.^{-1}$

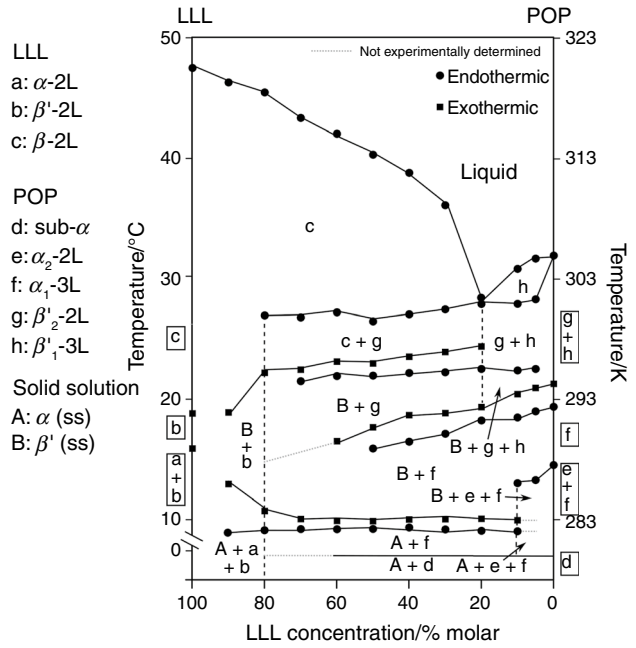


**Fig. 5** Phase behavior observed for LLL/PPO mixtures heated at 5 °C $min^{-1}$ after cooling at 25 °C $min^{-1}$. Delimited areas correspond to polymorphic domains between transitions experimentally determined

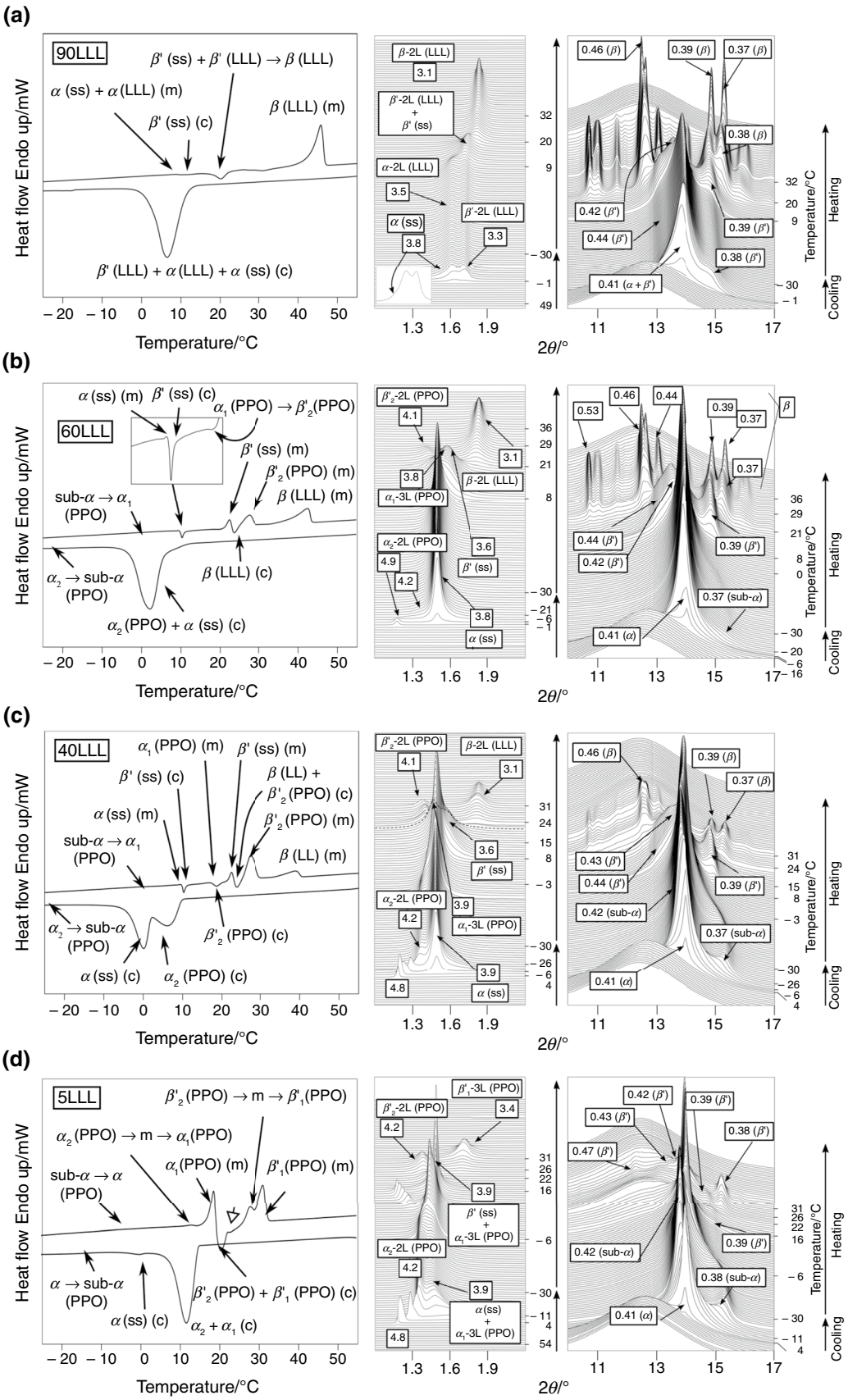
(a)
90LLL
β' (ss) + β' (LLL) → β (LLL)
α (ss) + α (LLL) (m)
β' (ss) (c)
β (LLL) (m)
β' (LLL) + α (LLL) + α (ss) (c)
Heat flow Endo up/mW
Temperature/°C
β-2L (LLL)
3.1
β'-2L (LLL) + β' (ss)
α-2L (LLL)
3.5
α (ss)
3.8
β'-2L (LLL)
3.3
0.46 (β)
0.39 (β)
0.37 (β)
0.38 (β)
0.42 (β')
0.44 (β')
0.39 (β')
0.38 (β')
0.41 (α + β')
Temperature/°C
Heating
Cooling
2θ/°
(b)
60LLL
α (ss) (m)
β' (ss) (c)
α1 (PPO) → β'2 (PPO)
β' (ss) (m)
β'2 (PPO) (m)
β (LLL) (m)
sub-α → α1 (PPO)
α2 → sub-α (PPO)
β (LLL) (c)
α2 (PPO) + α (ss) (c)
β'2-2L (PPO)
4.1
3.8
α1-3L (PPO)
α2-2L (PPO)
4.9
4.2
3.6
β' (ss)
3.8
α (ss)
3.1
β-2L (LLL)
0.53
0.46
0.44
0.39
0.37
β
0.37
0.44 (β')
0.42 (β')
0.39 (β')
0.37 (sub-α)
0.41 (α)
(c)
40LLL
α1 (PPO) (m)
β' (ss) (m)
β' (ss) (c)
β (LL) + β'2 (PPO) (c)
α (ss) (m)
β'2 (PPO) (m)
sub-α → α1 (PPO)
β (LL) (m)
α2 → sub-α (PPO)
β'2 (PPO) (c)
α (ss) (c)
α2 (PPO) (c)
β'2-2L (PPO)
4.1
β-2L (LLL)
3.1
3.6
β' (ss)
α2-2L (PPO)
3.9
4.2
α1-3L (PPO)
3.9
4.8
α (ss)
0.46 (β)
0.39 (β)
0.37 (β)
0.43 (β')
0.44 (β')
0.39 (β')
0.42 (sub-α)
0.37 (sub-α)
0.41 (α)
(d)
5LLL
β'2 (PPO) → m → β'1 (PPO)
α2 (PPO) → m → α1 (PPO)
α1 (PPO) (m)
β'1 (PPO) (m)
sub-α → α (PPO)
α → sub-α (PPO)
α (ss) (c)
β'2 (PPO) + β'1 (PPO) (c)
α2 + α1 (c)
β'1-3L (PPO)
β'2-2L (PPO)
3.4
4.2
3.9
β' (ss) + α1-3L (PPO)
α2-2L (PPO)
4.2
3.9
α (ss) + α1-3L (PPO)
4.8
0.42 (β')
0.39 (β')
0.43 (β')
0.38 (β')
0.47 (β')
0.42 (sub-α)
0.39 (β')
0.38 (sub-α)
0.41 (α)

◂**Fig. 6** LLL/PPO mixtures. DSC (left) and SR-XRD data (right) of **a** 90LLL/10PPO, **b** 60LLL/40PPO, **c** 40LLL/60PPO, and **d** 5LLL/95PPO mixtures heated at 5 °C $min^{-1}$ after cooling at 25 °C $min^{-1}$. (c): crystallization; (m): melting. *d*-spacing values are given in nm

peaks at 0.46, 0.39, and 0.37 nm). In blends with LLL content < 15%, single β-2L solid solutions were identified. Thus, in comparison with pure POP and PPO, molecular compound formation favored the solubility of LLL in the mixed-acid TAGs. Blends with 95–60% LLL content showed two melting events during heating associated with β-2L crystals rich in POP/PPO (in solid solution with LLL) and β-2L (LLL). In mixtures with 35% to 15% LLL, no β-2L (LLL) was detected by XRD. In turn, the peak at 3.3 nm (002 reflection) in SAXD patterns and those at 0.43, 0.40, and 0.37 nm in WAXD patterns were assigned to metastable δ-3L (POP). As shown by the diagram, the abrupt drop in melting temperature caused by the absence of LLL crystals led to the flattening of the liquidus curve toward the 50POP/50PPO sample. In addition, no distinct β-2L (ss) and δ-3L (POP) melting events could be discerned by DSC.

## Mixtures subjected to dynamic thermal treatments of cooling and reheating

Figure 8 summarizes the polymorphic behavior of LLL/(50POP/50PPO) mixtures cooled at 25 °C $min^{-1}$ to − 30 °C and subsequently heated at 5 °C $min^{-1}$. In a similar manner to LLL/POP and LLL/PPO mixtures, their crystallization and transformation varied according to the composition, and were governed by diverse metastable phases behaving in a eutectic manner at almost the whole range of compositions.

DSC curves obtained when cooling blends with 90 to 60% LLL content (Fig. 9) showed single exothermic peaks at ~2 to − 3 °C. According to SR-XRD data of the 90LLL/5POP/5PPO mixture (Fig. 9a), β′-2L (LLL) (peaks at 3.3, 0.44, and 0.39 nm), α-2L (LLL) (3.6 and 0.41 nm), and α (ss) (4.0 and 0.41 nm) crystallized. A lower LLL content promoted the formation of α (ss), which crystallized alone in the 60LLL/20POP/20PPO mixture (see Fig. 9c).

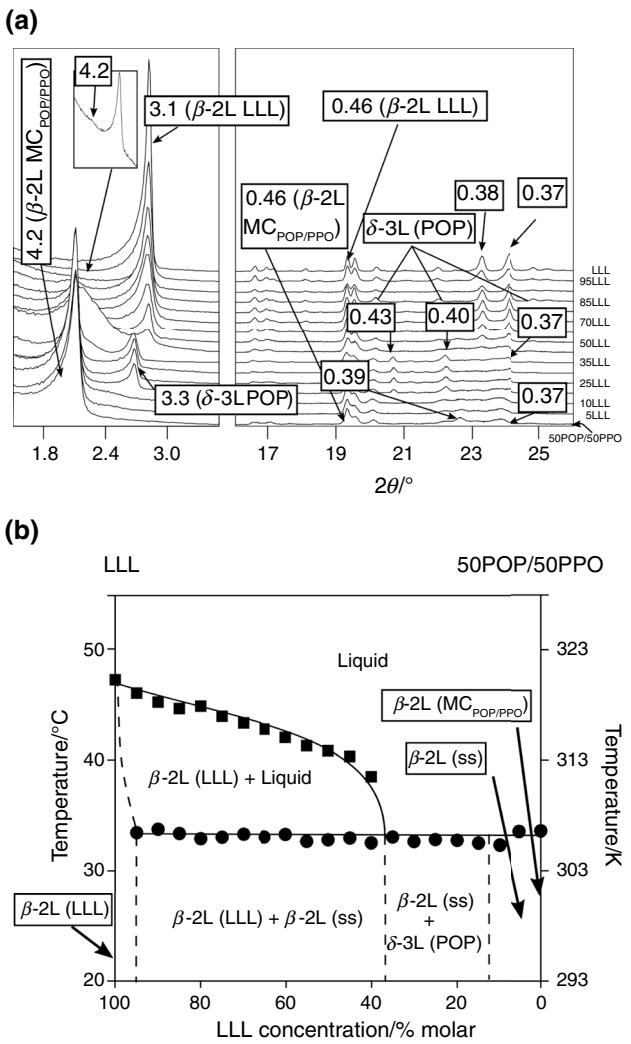


**Fig. 7** LLL/(50POP/50PPO) mixtures stabilized at 37 °C for 5 days and at 27 °C for 12 months. **a** XRD patterns obtained at 10 °C. *d*-spacing values are given in nm. **b** Phase diagram obtained when heating the mixtures at 2 °C $min.^{-1}$

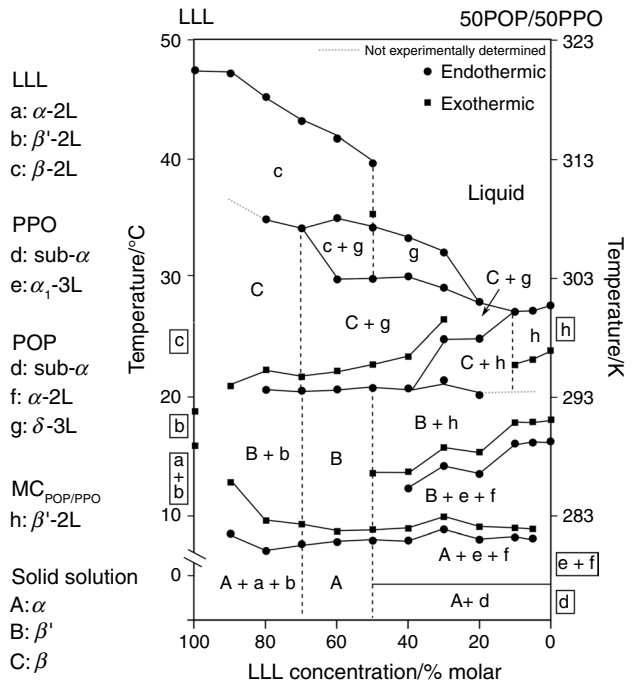


**Fig. 8** Phase behavior observed for LLL/(50POP/50PPO) mixtures heated at 5 °C $min^{-1}$ after cooling at 25 °C $min^{-1}$. Delimited areas correspond to polymorphic domains between transitions experimentally determined

When reheating these blends, α (ss) and α-2L (LLL) melted first, and β′ (ss) crystallized. In the 80LLL/10POP/10PPO mixture, endothermic and exothermic events were detected at ~ 7 and ~ 9 °C by DSC (Fig. 9b). Near these temperatures, related SAXD patterns revealed the vanishing of peaks at 4.0 and 3.6 nm. In parallel, one arose at 3.4 nm, and β′ WAXD reflections developed (0.44, 0.42, and 0.39 nm). The next melting of β′ (ss) (and some β′ of LLL) was followed by the crystallization of β with SR-XRD peaks at 3.1, 0.46, 0.39, and 0.37 nm (endothermic and exothermic events at ~ 21 and ~ 22 °C in the DSC curve). The shifting of the peak at 3.2–3.1 nm on further heating suggested that β′ (ss) transformed first into β (ss), then β (ss) melted (DSC peak at ~ 35 °C), and β-2L (LLL) (3.2 → 3.1 nm) occurred. In agreement, the 60LLL/20POP/20PPO blend (see Fig. 9c) showed the transition of β′ (ss) to a β (ss) form with a less sharp SAXD reflection of higher *d*-spacing value (peak at 3.3 nm detected at ~ 24 °C). WAXD peaks at 0.43 and 0.39 nm accompanying β ones after the transition indicated that some δ-3L (POP) (002 reflection at 3.3 nm) was also formed. In the DSC curve, the events involving from the melting of β (ss) to the final melting of δ-3L (POP) and β-2L (LLL) led to the complex thermal phenomena ranging from 25 to 45 °C.

Three DSC events were detected in mixtures rich in POP/PPO when cooling (see experimental data in Fig. 10). The energy and $T_{top}$ of the first and third ones grew toward the 5LLL/47.5POP/47.5PPO blend, whereas the second one was barely detected at the same. Based on SR-XRD data, α-2L (POP) crystallized first (SAXD peak at 5.0 nm → 4.6 nm and WAXD peak at 0.41 nm). Then, α (ss) occurred (SAXD peak at 4.0–4.1 nm) and $\alpha_1$-3L (PPO) formed next (diffuse SAXD peak at ~ 3.9 nm). Some $\alpha_2$-2L (PPO), with similar XRD patterns to α-2L (POP), may also have crystallized. The WAXD peak at 0.38 nm seen at ~ -20 °C revealed a α → sub-α transition. Given its absence in LLL-rich blends, this event probably only involved α crystals of POP and PPO.

When reheating, sub-α → α and α (ss) → melt → β′ (ss) transitions were succeeded by the melting of α-2L (POP) and $\alpha_1$-3L (PPO) at ~ 13 °C, after which β′-2L ($MC_{POP/PPO}$) crystallized. In accordance, peaks at 4.1, 0.44, 0.43, and 0.39 nm grew at a close temperature in SR-XRD patterns (see Fig. 10). On further heating, the broad DSC peak at ~ 21 °C in the 40LLL/30POP/30PPO blend (Fig. 10a) was due to the melting of β′ (ss) and β′-2L ($MC_{POP/PPO}$). Then, δ-3L (POP) and β (ss) crystallized at ~ 23 °C. β (ss) reflections (3.8 and 0.46 nm) vanished earlier from SR-XRD patterns, so this form melted before δ-3L (POP) (last DSC event at ~ 25 to ~ 40 °C). As shown for the 20LLL/40POP/40PPO mixture in Fig. 10b, δ-3L (POP) and β (ss) obtained from the β′ (ss) melt were barely identified and did not occur at decreasing LLL content. Even at a 5% LLL content (Fig. 10c), DSC peaks due to α (ss) melting and β′ (ss) crystallization were observed. Apart from this, the overall transformation behavior was ruled by POP/PPO. The α crystals of POP and PPO formed on cooling, melted at ~ 16 °C when reheating. Then, β′-2L ($MC_{POP/PPO}$) crystallized (DSC peak at ~ 17 to ~ 25 °C) and melted at ~ 27 °C without transform into stable β-2L ($MC_{POP/PPO}$).

## Discussion

The polymorphic behavior and solid miscibility of stable and metastable LLL/POP and LLL/PPO mixtures were evaluated to deepen insight into the eutectic interactions characterizing blends of lauric and non-lauric lipids. To assess the effect of promoting molecular compound formation in the final mixing behavior, LLL/(50POP/50PPO) mixtures were also investigated.

LLL/POP and LLL/PPO mixtures subjected to 9 months of stabilization at 27 °C displayed identical eutectic behavior. Both systems showed eutectic compositions with around 20–10% LLL content and no solubility of each TAG in the solid phase of the other at the lowest concentrations tested. The formation of TAG mixed crystals is affected by the lattice distortion caused by the incorporation of a guest TAG molecule into the lattice of chemically different host TAG molecules, which greatly depends on the presence of *cis*-unsaturated bonds and differences in chain length [30]. Thus, the high incompatibility found in LLL/POP and LLL/PPO mixtures (mutual solubility < 5%) was related to steric hindrance between saturated and unsaturated fatty acid chains (see molecular models in Fig. 11 [31]). In addition, the different lengths of lauric and palmitic acid moieties (12 and 16 carbon atoms, respectively) of TAG components would also contribute to phase separation by increasing the instability at methyl end regions. In line with the previous results on stable PPP/POP and PPP/PPO mixtures [5, 32], the varying symmetry and polymorphism of POP and PPO did not substantially change the final mixing properties.

As reflected in the crystalline maps constructed for LLL/POP and LLL/PPO mixtures (Fig. 2 and 5), during dynamic thermal treatments, α (ss) always crystallized on cooling. However, α phases very rich in one of the TAGs were also formed at all or almost all ratios, even at the lowest concentrations tested. There is experimental evidence that solid solution formation is kinetically favored at high supercooling conditions. This was observed in PPP/SSS, PPP/POP, PPP/PPO, or PPP/POO mixtures cooled at rates ≥ 25 °C $min^{-1}$ [4, 26, 33], which tend to phase separation at decreasing speed of cooling [3, 5, 34–36]. In LLL/POP and LLL/PPO mixtures, the positive excess free energy of mixing that would prevent miscibility was partially overcome due to the fast-cooling conditions. Furthermore, the single α (ss) phases obtained in LLL/POP mixtures near the equimolecular

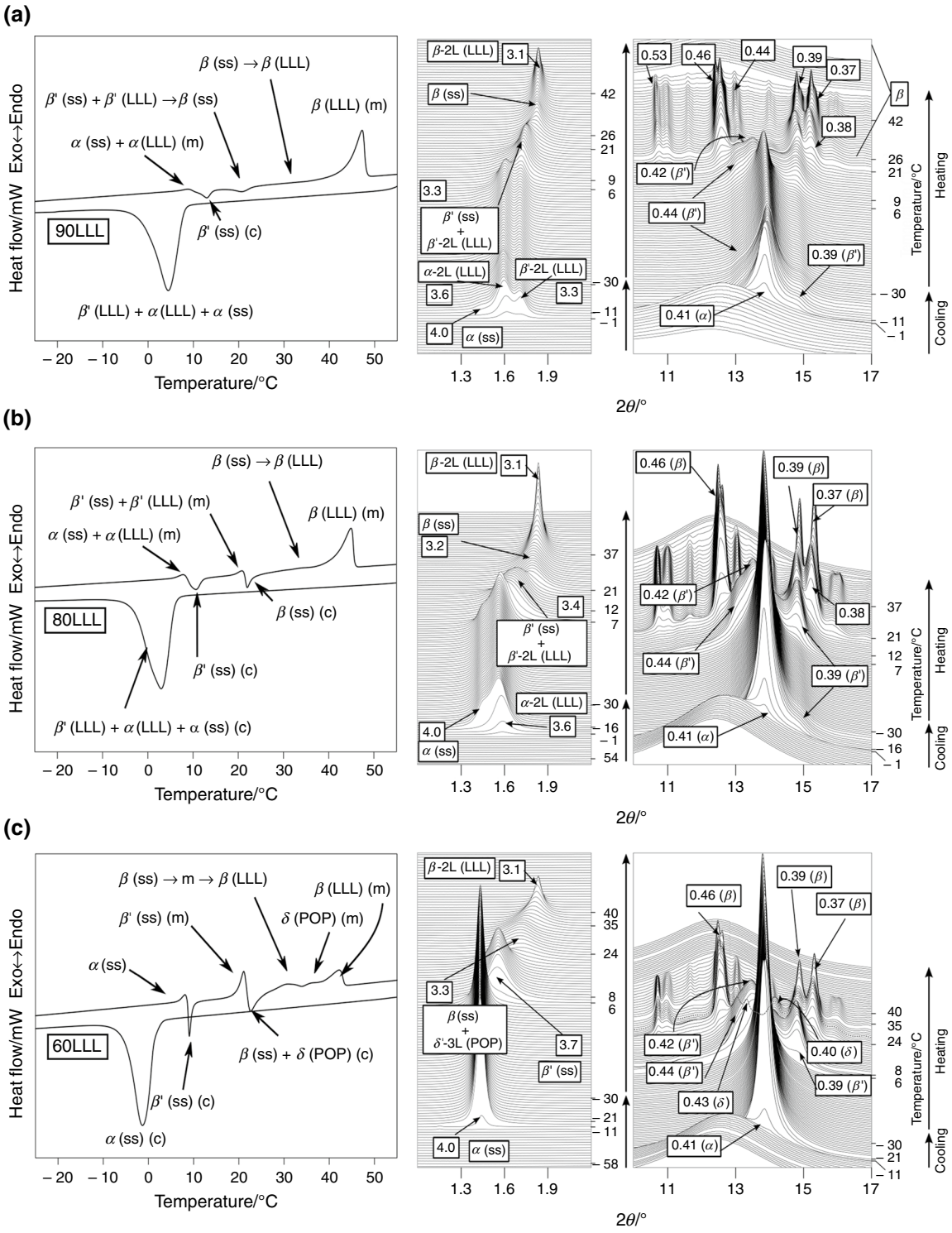


**Fig. 9** LLL/(50POP/50PPO) mixtures. DSC (left) and SR-XRD data (right) of **a** 90LLL/5POP/5PPO, **b** 80LLL/10POP/10PPO, and **c** 60LLL/20POP/20PPO mixtures heated at 5 °C $min^{-1}$ after cooling at 25 °C $min^{-1}$. (c): crystallization; (m): melting. *d*-spacing values are given in nm

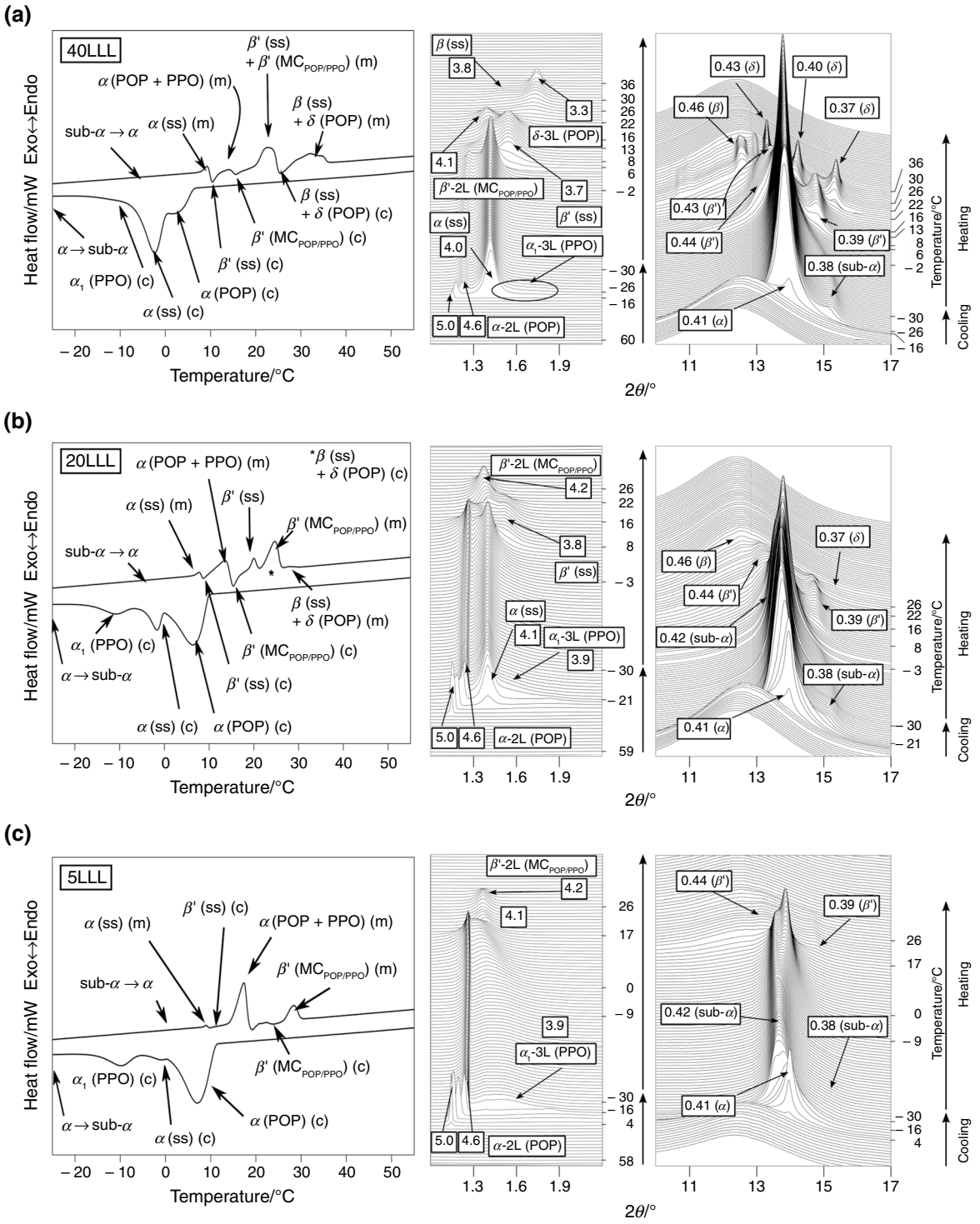


**Fig. 10** LLL/(50POP/50PPO) mixtures. DSC (left) and SR-XRD data (right) of **a** 40LLL/30POP/30PPO, **b** 20LLL/40POP/40PPO, and **c** 5LLL/47.5POP/47.5PPO mixtures heated at 5 °C $min^{-1}$ after cooling at 25 °C $min^{-1}$. (c): crystallization; (m): melting. *d*-spacing values are given in nm

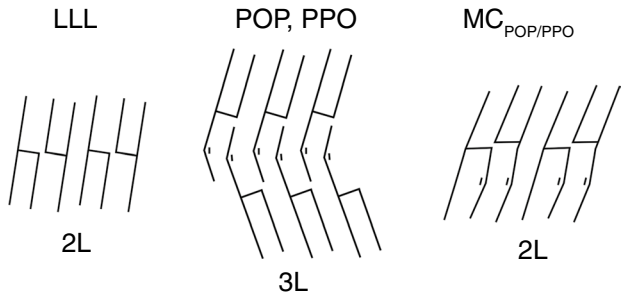


**Fig. 11** Structural models of TAGs included in the present study

composition (see Fig. 2) could be due to a growing steric hindrance at an equal ratio of TAGs in the samples. This would hinder the molecular packing, cause a decrease in the crystallization temperature and, thus, ease the formation of low-order solid solutions in the α form. Despite this, melt-mediated α (ss) → β′ (ss) transitions and β′ (ss) melting when reheating were always followed by phase separation. The next polymorphic crystallization and transformation behavior varied as a function of the major TAG present in the blends.

The results on LLL/POP and LLL/PPO mixtures relate directly to the functionality of products like margarine based on palm (rich in POP) and palm kernel (rich in LLL) oils. Their blends tend to immiscibility, with eutectic formation at ~40% palm kernel oil content [12, 37]. This behavior is valuable to obtain products with butter-like properties like plasticity and a soft mouthfeel [13, 38]. The high immiscibility of LLL and POP also links to the low compatibility of CB (rich in POS, SOS, and POP) and lauric-CBS. In this connection, LLL/SOS mixtures aged for two weeks at 25 °C showed a solubility of LLL in SOS < 10%, and of SOS in LLL < 3% [20].

In contrast to the binary systems, no polymorphic stability was achieved at all ratios in LLL/(50POP/50PPO) mixtures incubated for one year. β-2L solid solutions occurred at LLL content < 15%. The higher solubility of LLL in the mixed-acid TAGs compared with the binary systems could be due to the double chain-length structure promoted in POP/PPO mixtures when forming $MC_{POP/PPO}$ (Fig. 11). Since the oleic acid content in the system did not vary from binary to ternary mixtures, one may consider that in triple structures of stable POP and PPO, larger voids in the crystalline structure when including shorter LLL molecules could lead to greater instability at methyl end regions. The polymorphism observed in mixtures at 35–15% LLL content indicated that increasing the amount of LLL altered the typical 1:1 interaction of POP and PPO in $MC_{POP/PPO}$. Thus, β-2L (ss) was concurrently present with δ-3L (POP) at these compositions. During experiments under varying cooling/heating rates, mixtures with 60 to 20% LLL content also showed the occurrence of these forms after the melting of β′ (ss). Specifically, in the 40LLL/30POP/30PPO mixture (see Fig. 10), β (ss) and δ-3L (POP) melted directly without further crystallization events. By contrast, the same sample subjected to thermodynamic stabilization showed separate LLL in the β-2L form. This means that, despite the low molecular diffusivity in the solid state presumed for the incubated mixtures, an eventual separation of LLL may be also expected in mixtures with LLL content ≤ 35%. The long lifespan of β (ss) and δ-3L (POP) could relate to a narrow difference in the free energy of the system in such state and in most stable forms. This would reduce the driving force for the polymorphic transformation and, therefore, slow the stabilization. Despite the expected separation of LLL from POP and PPO, the possibility of obtaining highly-stable solid solutions of these three components shows triacylglycerols forming molecular compound as a promising strategy to increase the current applications of lauric oils and their fractions. Concretely, promoting this kind of ternary interaction could be useful to avoid unwanted properties in food products caused by eutectic formation, such as softening effects or fat bloom development in chocolate-type products.

## Conclusions

LLL/POP and LLL/PPO mixtures showed full immiscibility in the stable state and a clear tendency to eutectic interaction also in the metastable state. Likewise, phase separation prevailed in LLL/(50POP/50PPO) mixtures but it was confirmed that: (i) the solubility of LLL in POP and PPO improved when both TAGs were forming a β-2L structure of MC crystals of POP/PPO and (ii) the formation of long-life solid solutions including more than 10% LLL content entailed the separation of some POP. However, to what extent the 1:1 ratio of POP and PPO in $MC_{POP/PPO}$ was altered in three-component solid solutions and the specific interactions triggering this behavior remain unclear. These issues could be further clarified by evaluating the crystalline behavior of LLL/POP/PPO mixtures at varying the POP/PPO ratio. The engineering of solid solutions of lauric-based TAGs and unsaturated TAGs with longer saturated fatty acids, such as palmitic or stearic, could be of practical value in lipid structuring applications. i.e., for the development of β-stable lauric-rich CB alternatives displaying higher compatibility with CB than the currently available lauric-CBS.

**Supplementary Information** The online version contains supplementary material available at https://doi.org/10.1007/s10973-023-12421-9.

**Acknowledgements** This work was supported by the Generalitat de Catalunya through project 2021 SGR 00262 and Grant PID-2019-107032RB-I00 funded by MCIN/

AEI/10.13039/501100011033. J.M received financial support from MCIN/AEI/10.13039/501100011033 and ''ESF Investing in your future'' through grant BES-2016-076612. The authors thank the funding from Alba synchrotron facility for performing the SR-XRD experiments (proposal 2020074400) and the help of Dr. Marc Malfois at beamline BL11-NCD-SWEET.

**Author contributions** All authors contributed to the study conception and design. Research materials preparation, experiments, data acquisition and analyses, and original draft preparation were carried out by JM. Manuscript review and funding acquisition were performed by LB-G. and TC.

**Funding** Open Access funding provided thanks to the CRUE-CSIC agreement with Springer Nature.

## Declarations

**Conflict of interest** The authors have no competing interests to declare that are relevant to the content of this article.



## References

1. Timms RE. Confectionery fats handbook. In: Timms RE, editor. Properties, production and application. Bridgwater: The Oily Press; 2003.
2. Zhang L, Ueno S, Sato K. Binary phase behavior of saturated-unsaturated mixed-acid triacylglycerols—a review. J Oleo Sci. 2018;67:679–87.
3. Minato A, Ueno S, Yano J, Wang ZH, Seto H, Amemiya Y, et al. Synchrotron radiation X-ray diffraction study on phase behavior of PPP–POP binary mixtures. J Am Oil Chem Soc. 1996;73:1567–72.
4. Gibon V, Durant F. Etude du polymorphisme et de l'intersolubilite de triglycerides palmito-oleiques par diffraction rx de poudres et analyse calorimetrique differentielle. Bull Soc Chim Belges. 1985;94:1009–20.
5. Macridachis J, Bayés-García L, Calvet T. Solid phase behavior of mixture systems based on tripalmitoyl glycerol and monounsaturated triacylglycerols forming a molecular compound. Phys Chem Chem Phys. 2022;24:3749–60.
6. Minato A, Ueno S, Smith K, Amemiya Y, Sato K. Thermodynamic and kinetic study on phase behavior of binary mixtures of POP and PPO forming molecular compound systems. J Phys Chem B. 1997;101:3498–505.
7. Marikkar JMN, Saraf D, Dzulkifly MH. Effect of fractional crystallyzation on composition and thermal behavior of coconut oil. Int J Food Prop. 2013;16:1284–92.
8. Eskin NAM, List GR. Food applications of lipids. In: Akoh CC, editor. Food lipids: chemistry, nutrition, and biotechnology. 4th ed. Boca Raton: CRC Press; 2017. p. 421–52.
9. Talbot G. Compound coatings. In: Talbot G, editor. Science and technology of enrobed and filled chocolate, confectionery, and bakery products. Cambridge: CRC Press; 2009. p. 80–100.
10. Shukla VK. Confectionery lipids. In: Shahidi F, editor. Bailey's industrial oil and fat products. 6th ed. Hoboken: Wiley; 2005. p. 159–74.
11. Smith KW. Confectionery fats. In: Garti N, Widlak NR, editors. Cocoa butter and related compounds. Urbana: AOCS Press; 2012. p. 475–96.
12. Norlida HM, Ali ARM, Muhadhir I. Blending of palm oil, palm stearin and palm kernel oil in the preparation of table and pastry margarine. Int J Food Sci Nutr. 1996;47:71–4.
13. Liu C, Meng Z, Chai X, Liang X, Piatko M, Campbell S, et al. Comparative analysis of graded blends of palm kernel oil, palm kernel stearin and palm stearin. Food Chem. 2019;286:636–43.
14. Liu C, Meng Z, Cao P, Jiang J, Liang X, Piatko M, et al. Visualized phase behavior of binary blends of coconut oil and palm stearin. Food Chem. 2018;266:66–72.
15. Hartel RW, von Elbe JH, Hofberger R. Confectionery science and technology. Gewerbestrasse: Springer international Publishing; 2018.
16. Silva TJ, Barrera-Arellano D, Ribeiro APB. Margarines: Historical approach, technological aspects, nutritional profile, and global trends. Food Res Int. 2021;147: 110486.
17. Gordon MH, Padley FB, Timms RE. Factors influencing the use of vegetable fats in chocolate. Fette Seifen Anstrichm. 1979;81:116–21.
18. Talbot G. Vegetable fats. In: Beckett ST, editor. Industrial chocolate manufacture and use. 4th ed. Oxford: Wiley-Blackwell; 2009. p. 415–33.
19. Macridachis-González J, Bayés-García L, Calvet T. An insight into the solid-state miscibility of triacylglycerol crystals. Molecules. 2020;25:4562.
20. Yoshikawa S, Watanabe S, Yamamoto Y, Kaneko F. Binary phase behavior of 1,3-distearoyl-2-oleoyl-sn-glycerol (SOS) and trilaurin (LLL). Molecules. 2020;25:5313.
21. Yoshikawa S, Watanabe S, Yamamoto Y, Kaneko F, Sato K. Interactive polymorphic crystallization behavior in eutectic triacylglycerol mixtures containing molecular compound crystals. Cryst Growth Des. 2022;22:1753–63.
22. Foubert I, Vanrolleghem PA, Thas O, Dewettinck K. Influence of chemical composition on the isothermal cocoa butter crystallization. J Food Sci. 2004;69:478–87.
23. Braipson-Danthine S, Gibon V. Comparative analysis of triacylglycerol composition, melting properties and polymorphic behavior of palm oil and fractions. Eur J Lipid Sci Technol. 2007;109:359–72.
24. Bayés-García L, Calvet T, Cuevas-Diarte MÀ, Ueno S. From trioleoyl glycerol to extra virgin olive oil through multicomponent triacylglycerol mixtures: crystallization and polymorphic transformation examined with differential scanning calorimetry and X-ray diffration techniques. Food Res Int. 2017;99:476–84.
25. PerkinElmer. Instructions model DSC-4. Norwalk: PerkinElmer; 1982.
26. Takeuchi M, Ueno S, Sato K. Synchrotron radiation SAXS/WAXS study of polymorph-dependent phase behavior of binary mixtures of saturated monoacid triacylglycerols. Cryst Growth Des. 2003;3:369–74.
27. Mizobe H, Tanaka T, Hatakeyama N, Nagai T, Ichioka K, Hondoh H, et al. Structures and binary mixing characteristics of enantiomers of 1-oleoyl-2,3-dipalmitoyl-sn-glycerol (S-OPP) and 1,2-dipalmitoyl-3-oleoyl-sn-glycerol (R-PPO). J Am Oil Chem Soc. 2013;90:1809–17.

28. Mykhaylyk OO, Martin CM. Effect of unsaturated acyl chains on structural transformations in triacylglycerols. Eur J Lipid Sci Technol. 2009;111:227–35.
29. Sato K, Arishima T, Wang ZH, Okima K, Sagi N, Mori H. Polymorphism of POP and SOS. I. Occurrence and polymorphic transformation. J Am Oil Chem Soc. 1989;66:664–74.
30. Wesdorp LH, Van Meeteren JA, de Jong S, van der Giessen R, Overbosch P, Grootscholten PAM, et al. Liquid–multiple solid phase equilibria in fats. Theory and experiments. In: Marangoni AG, Wesdorp LH, editors., et al., Structure and properties of fat crystal networks. 2nd ed. Boca Raton: CRC Press; 2013. p. 241–418.
31. Minato A, Yano J, Ueno S, Smith K, Sato K. FT–IR study on microscopic structures and conformations of POP–PPO and POP–OPO molecular compounds. Chem Phys Lipids. 1997;88:63–71.
32. Macridachis J, Bayés-García L, Calvet T. Mixing phase behavior of tripalmitin and oleic-rich molecular compound-forming triacylglycerols. Ind Eng Chem Res. 2021;60:5374–84.
33. Gibon V, Durant F, Deroanne C. Polymorphism and intersolubility of some palmitic, stearic and oleic triglycerides: PPP, PSP and POP. J Am Oil Chem Soc. 1986;63:1047–55.
34. Zhang L, Ueno S, Miura S, Sato K. Binary phase behavior of 1,3-dipalmitoyl-2-oleoyl-sn-glycerol and 1,2-dioleoyl-3-palmitoyl-rac-glycerol. J Am Oil Chem Soc. 2007;84:219–27.
35. Bayés-García L, Calvet T, Cuevas-Diarte MÀ, Ueno S, Sato K. Phase behavior of binary mixture systems of saturated-unsaturated mixed-acid triacylglycerols: effects of glycerol structures and chain-chain interactions. J Phys Chem B. 2015;119:4417–27.
36. Himawan C, MacNaughtan W, Farhat IA, Stapley AGF. Polymorphic occurrence and crystallization rates of tristearin/tripalmitin mixtures under non-isothermal conditions. Eur J Lipid Sci Technol. 2007;109:49–60.
37. Grimaldi R, Aparecida L, Gonçalves G, Gioielli LA. Interactions in interesterified palm and palm kernel oils mixtures. I-solid fat content and consistency. Grasas Aceites. 2001;52:349–54.
38. O'Brien RD. Fats and oils. In: O'Brien RD, editor. Formulating and processing for applications. 3rd ed. Boca Raton: CRC Press; 2009.